JMEPEG (2011) 20:1563–1568
DOI: 10.1007/s11665-011-9840-4

1059-9495/$19.00

Bonding Mechanisms and Shear Properties of Alumina Ceramic/Stainless Steel Brazed Joint

G.W. Liu, G.J. Qiao, H.J. Wang, J.P. Wang, and T.J. Lu

(Submitted June 9, 2010; in revised form September 17, 2010)

Al_2O_3 ceramic/stainless steel joints were fabricated by activated molybdenum-manganese (Mo-Mn) sintering metallization plus vacuum brazing using Ag-28 wt.% Cu alloy. The bonding mechanisms including metallization and interfacial bonding were analyzed and discussed by means of scanning electron microscopy (SEM), energy dispersive spectroscopy (EDS), and x-ray diffraction (XRD). Tests were also carried out to examine the influence of brazing on joint shear strength. The metallization mechanisms of glassy phase migration and chemical reaction were confirmed experimentally, while Ni coating was found to play a key role in the joining of metallized ceramic to metal via the Ag-Cu filler layer. As a result of the joining, the average shear strength of the joints exceeds 95 MPa, with the maximum reaching 110 MPa.

Keywords alumina ceramic, bonding mechanism, brazing, mechanical property, metallization

1. Introduction

Ceramic/metal joining has been envisioned as a feasible way to overcome the brittleness and poor machinability of ceramic materials, as well as the difficulty in the fabrication of complex-shaped and large-sized ceramic components. The joining of high-purity Al_2O_3 ceramics has now become a well-established practice, including the sintering metal powder process (Mo-Mn process) (Ref 1-4), active metal brazing (Ref 4, 5), and the partial transient liquid phase (PTLP) technique (Ref 6, 7). Compared with the conventional Mo-Mn process, activated Mo-Mn process is more commonly used in industry for high-purity Al_2O_3 ceramic-metal seals, with metallizing formula added with active agent, such as Al_2O_3 and SiO_2.

A typical Mo-Mn process includes three key steps: ceramic sintering metallization, secondary metallization (nickel plating and subsequent annealing), and vacuum brazing. The fracture strength and reliability of the resulting joint in ceramic-metal seals are of particular concern, affected mainly by the metallizing formula, the sintering process of the metallization, the brazing conditions, and the characteristics of ceramic matrix and metal component. These factors correlate closely with the bonding mechanisms and interlayer residual thermal stresses, and hence influence the joint mechanical properties. It has been established that the mechanisms of the conventional Mo-Mn metallization mainly include chemical reaction (Ref 8) and glassy phase migration (Ref 9, 10). However, differences in the metallization mechanisms exist between the conventional and activated Mo-Mn metallization (Ref 11), especially in the direction of glassy phase migration, and hence the mechanisms of metallization and interfacial bonding and their influence on bonding strength need to be further explored. This work aims to investigate the activated Mo-Mn metallization mechanisms of high-purity Al_2O_3 ceramic, to examine the interfacial microstructure of Al_2O_3 ceramic/stainless steel joints, and to quantify the influence of brazing cooling rate on joint shear strength.

G.W. Liu and **T.J. Lu**, MOE Key Laboratory for Strength and Vibration, Xi'an Jiaotong University, Xi'an 710049, China; and **G.J. Qiao, H.J. Wang,** and **J.P. Wang**, State Key Laboratory for Mechanical Behavior of Materials, Xi'an Jiaotong University, Xi'an 710049, China. Contact e-mails: gwliu76@mail.xjtu.edu.cn, gjqiao@mail.xjtu.edu.cn, and tjlu@mail.xjtu.edu.cn.

2. Experimental

2.1 Materials and Sample Preparation

The powder selected contains 98% Al_2O_3, 1% SiO_2, and 1% MgO (wt.%, same below) after mixing and milling. The Al_2O_3 powder used (Zibo Hengjitianli Industry and Business Co., Ltd, China) is high purity and super-fine, 99.95% purity and average particle size ~0.5 μm. The green bodies were sintered in air at 1600 °C for 2.5 h after mold forming, with linear pressing up to 200 MPa for 30 s. Cylindrical 98% Al_2O_3 ceramic pieces having sizes of ∅ 18 × 6 mm were obtained, with apparent porosity, bulk density (measured by the Archimedes method), and bending strength about 1.5%, 3.74 g/cm^3, and 330 MPa, respectively. Figure 1 shows the microstructure of a polished sample after thermal etching (slowly heating to 1500 °C for 30 min in air), which indicates average grain size of about 10 μm. Commercially available stainless steel (AISI 304, S-S) with dimensions of ∅ 10 × 5 mm was used as the metal component for joining, with chemical composition: 0.050% C, 0.433% Si, 1.152% Mn, 0.022% P, 0.002% S, 17.32% Cr, 8.16% Ni, 0.201% Cu, and Fe (balance). Ag-28% Cu (Ag-Cu) alloy preform, diameter 0.8 mm and melting point 780 °C, was used as the filler metal. The average linear coefficient of thermal expansion (CTE, 20-600°C) is about 7.4×10^{-6}/°C for Al_2O_3 and 18.5×10^{-6}/°C for S-S (Ref 12). The metallizing formula was composed of 70% Mo and 30% active agent, consisting of 40% MnO, 35% Al_2O_3, and 25% SiO_2. After milling with roller for 80 h, the particle size distribution in the

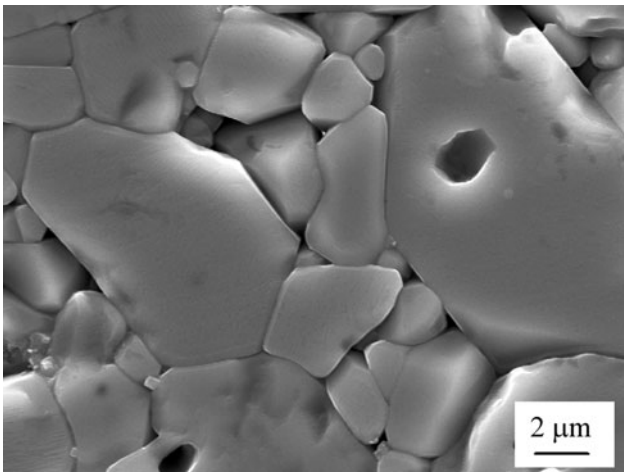

Fig. 1 Microstructure of 98% Al_2O_3 ceramic sample

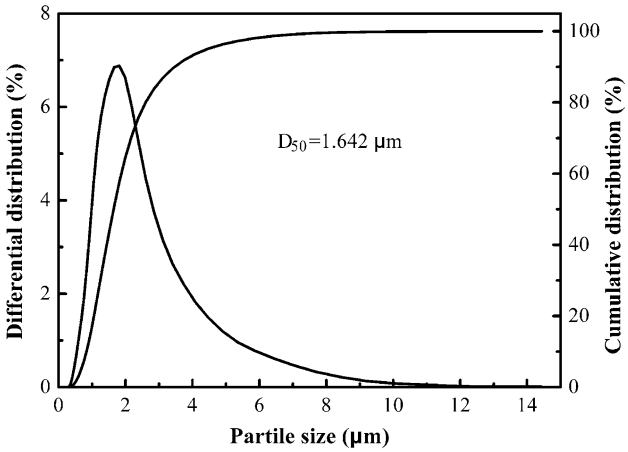

Fig. 2 Particle size distribution curves of metallizing formula powder after milling

metallizing formula powder displayed a meso-diameters D_{50} of 1.642 μm, as shown in Fig. 2.

Before the sintering metallization was applied, the Al_2O_3 ceramic samples, annular Ag-Cu alloy performs and S-S columns were carefully cleaned. This procedure includes three steps: boiling in alkalescent scouring agent (NaOH 30 g/L + Na_2CO_3 20 g/L + Na_2SiO_3 10 g/L + OP-10(emulsifier) 3 g/L + $Na_3PO_4 \cdot 12H_2O$ 50 g/L) for 20 min, rinsing with distilled water and finally ultrasonic cleaning in acetone. The metallizing paste was prepared from the metallizing formula powder, diethyl oxalate, and collodion by ultrasonic vibrating and stirring. One side of the Al_2O_3 sample surfaces was painted with the metallizing paste and then air-dried. The metallization was then sintered to the ceramic in a high-temperature H_2 furnace (atmosphere: 0.01 MPa H_2) at a heating rate less than 10 °C/min to 1500 °C which was maintained for 60 min, and then cooling slowly to the room temperature. In order to help the Ag-Cu alloy wet the metallizing surface, a thin Ni layer was coated on the brazing surface of the metallized Al_2O_3 ceramic by electro-plating in Watts' solution ($NiSO_4$ 280 g/L + $NiCl_2$ 45 g/L + HBO_3 35 g/L + $C_{12}H_{25}SO_4Na$ 0.1 g/L) at a current density about 1 A/dm^2 for 40 min. The plating was subsequently annealed at 1000 °C for 60 min in vacuum

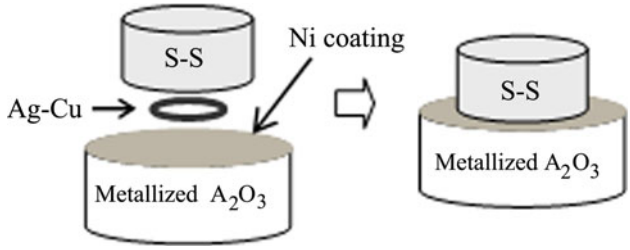

Fig. 3 Schematic of brazing assembly

($\sim 8 \times 10^{-3}$ Pa). The metallized ceramic pieces with two metallizing coatings (Mo-Mn and Ni), annular Ag-Cu alloy preforms and S-S columns were assembled as shown in Fig. 3, then brazed at 820 °C for 20 min in a vacuum furnace at about 8×10^{-3} Pa.

2.2 Sample Characterization

The shear strength of the brazed joint was measured using an Instron-1195 universal test system at a loading speed of 0.5 mm/min (Ref 13). The mean value of the joint shear strength for each brazing condition was the arithmetical average of five joint strength measurements.

Selected metallized ceramic and Al_2O_3/S-S joint were cut off along the direction perpendicular to the sintered coating or joint line, and then polished. The microstructures of the metallized ceramic and joint cross section were examined using scanning electron microscopy (SEM, Model JSM-7000F, JEOL, Japan). Energy dispersive spectroscopy (EDS, Model Oxford INCA, UK) was employed to determine the elemental compositions and their distribution. The phase compositions of the metallizing formula and the Mo-Mn metallizing layer were identified by x-ray diffraction (XRD, Model X'Pert PRO, PANalytical, Ltd., Holland) analysis at 40 kV and 40 mA using Cu K_α radiation.

3. Results and Discussion

3.1 Metallization Mechanisms

Figure 4 displays the SEM micrographs of a Mo-Mn metallized Al_2O_3 ceramic cross section. A porous sintered coating, ~50 μm thick, acted as the metallizing layer (i.e., Mo-Mn layer) that attached tightly to the ceramic matrix. A degenerative ceramic layer was seen to exist between the Al_2O_3 ceramic matrix and the sintered coating, i.e., between the vertical black lines marked in Fig. 4(a). The degenerative ceramic layer with a thickness of ~15 μm was mainly composed of big Al_2O_3 grains and glassy phases (the reaction products between MnO, Al_2O_3, and SiO_2) that migrated from the sintered coating (Fig. 4b), and is referenced as the transition layer. Moreover, according to the elemental EDS profiles across the metallized ceramic cross section, both Al and oxygen profiles exhibited a descending trend from the ceramic matrix across the transition layer (Ref 3). This indicates that certain matters with lower contents of Al and oxygen than that of Al_2O_3, such as MnO, SiO_2 or the reaction products between MnO, Al_2O_3, and SiO_2, had entered into the ceramic matrix to form the transition layer, i.e., glassy phases migrated from the metallizing layer to the ceramic matrix (Ref 3). By comparison, in the conventional Mo-Mn metallization process, glassy

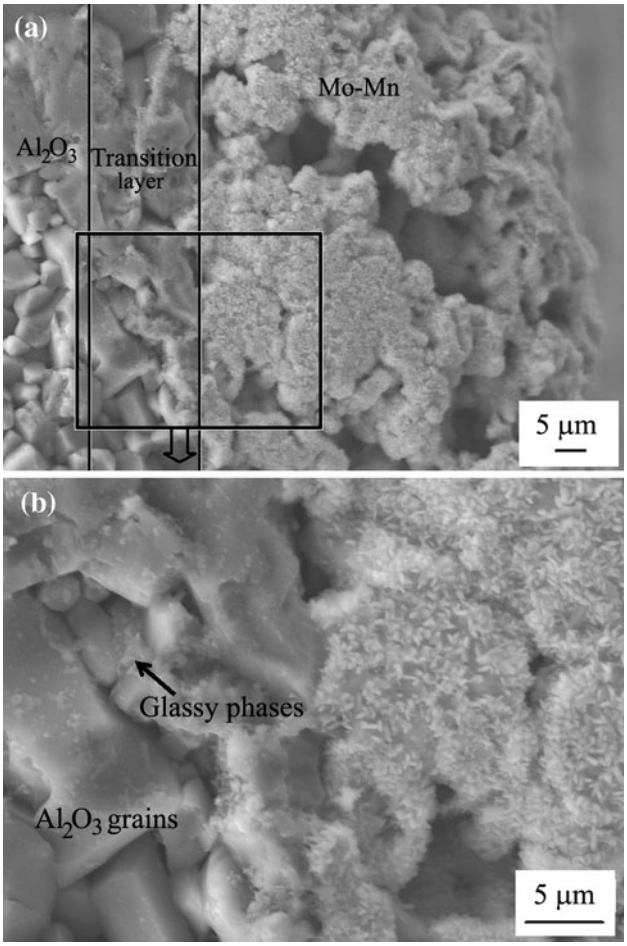

Fig. 4 SEM micrographs of (a) metallized Al_2O_3 ceramic cross section and (b) Al_2O_3/Mo-Mn interface

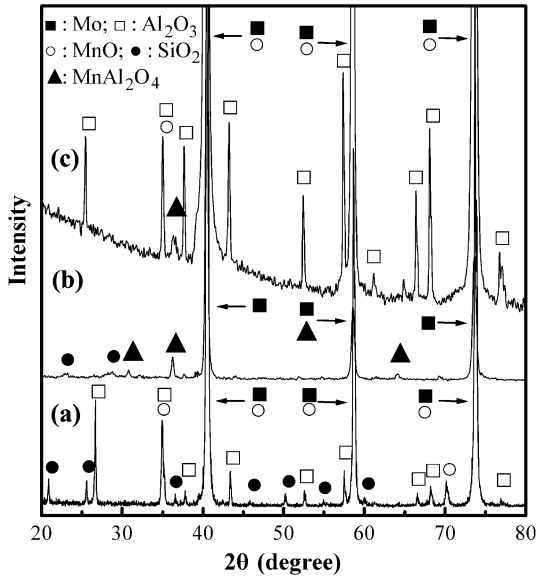

Fig. 5 XRD patterns of (a) metallizing formula powder, (b) sintered body of metallizing formula powder, and (c) Mo-Mn layer

phases originate in the Al_2O_3 ceramic matrix or reaction products between the ceramic matrix and MnO, and migrate inversely from the ceramic matrix to the metallizing layer (Ref 9, 10). Therefore, the glassy phase migration observed in the present study was one of the activated Mo-Mn metallization mechanisms, with its direction running from the metallizing layer to the ceramic matrix.

To investigate the phase compositions and reaction products in the Mo-Mn layer, the metallized ceramic sample, the metallizing formula powder, and its sintered body (after mold forming and sintering under the same condition as the ceramic metallization process) were analyzed by means of XRD. From the XRD patterns shown in Fig. 5, it can be seen from curve (a) that the metallizing formula powder was composed of Mo, MnO, Al_2O_3, and SiO_2, while the $MnAl_2O_4$ phase appeared in both the curves (b) and (c). This indicates that, during the sintering of the metallization, MnO mainly reacted with Al_2O_3 in the metallizing formula to form $MnAl_2O_4$. By comparison, in the conventional Mo-Mn metallization process, $MnAl_2O_4$ is formed by chemical reaction between MnO and Al_2O_3 originated from the ceramic matrix. Furthermore, Al_2O_3 and MnO were not found in the sintered body, and the content of SiO_2 was very low as shown in curve (b), which suggests full reactions had occurred between Al_2O_3, MnO, and SiO_2 due to good contact on the mold forming. However, in the Mo-Mn metallizing layer, Al_2O_3 was found clearly, and traces of MnO and $MnAl_2O_4$ were also detected, but no SiO_2 existed, as shown in cure (c). A reasonable explanation is that the reactions may not have carried out fully between the active agent (MnO, Al_2O_3, and SiO_2) and the partial Al_2O_3 derived from the ceramic matrix.

Therefore, both glassy phase migration and chemical reaction were experimentally confirmed in the activated Mo-Mn metallization of high-Al_2O_3 ceramic.

3.2 Interfacial Bonding

The backscattered electron (BSE) images of the Al_2O_3/S-S joint cross section are presented in Fig. 6, focusing on six different regions of the section: the Al_2O_3 ceramic matrix, transition layer, Mo-Mn layer, Ni coating, Ag-Cu filler layer, and stainless steel (S-S) matrix. The Mo-Mn layer was mainly composed of black, dark, gray, and white phases (Fig. 6a). While the black and white phases were identified as the hole and the Mo-rich phase, respectively, the dark and gray phases mainly contained elements (Mn, Al, Si, and oxygen) in the active agent. The transition layer was formed by inter-reactions (chemical reaction and migration) between the ceramic matrix and the active agent during the sintering. Ni coating, about 4-9 μm thick, was present between the Mo-Mn layer and the Ag-Cu layer. The Ag-Cu layer joined the metallized ceramic to stainless steel via the two metallizing coatings: Mo-Mn layer and Ni coating. Besides the white Ag-rich phase (elemental Ag or Ag-Cu eutectic), a few black dots existed in the Ag-Cu layer, which, by EDS analysis, contained Cu and Ni near the Ni coating side or Cu, Ni, and Fe near the S-S side. In addition, a "sawtooth" appeared on the Ag-Cu/S-S interface due to the rough ground surface of S-S, which can contribute to the mutual bonding, and the Ag-Cu filler entered fully into the cavities of the "sawtooth," as shown Fig. 6(d).

To determine the elemental distribution at the Ni/Ag-Cu and Ag-Cu/S-S interfaces, EDS analysis by the line-scanning mode was adopted. Figure 7 shows the EDS profiles of the main elements across the Ag-Cu filler layer. Both sides of the Ag-Cu layer had a Cu-rich layer, 5-10 μm thick, but it proved difficult for the Ag element to enter the Ni coating. One possible reason for the formation of the two Cu-rich layers was that Ag

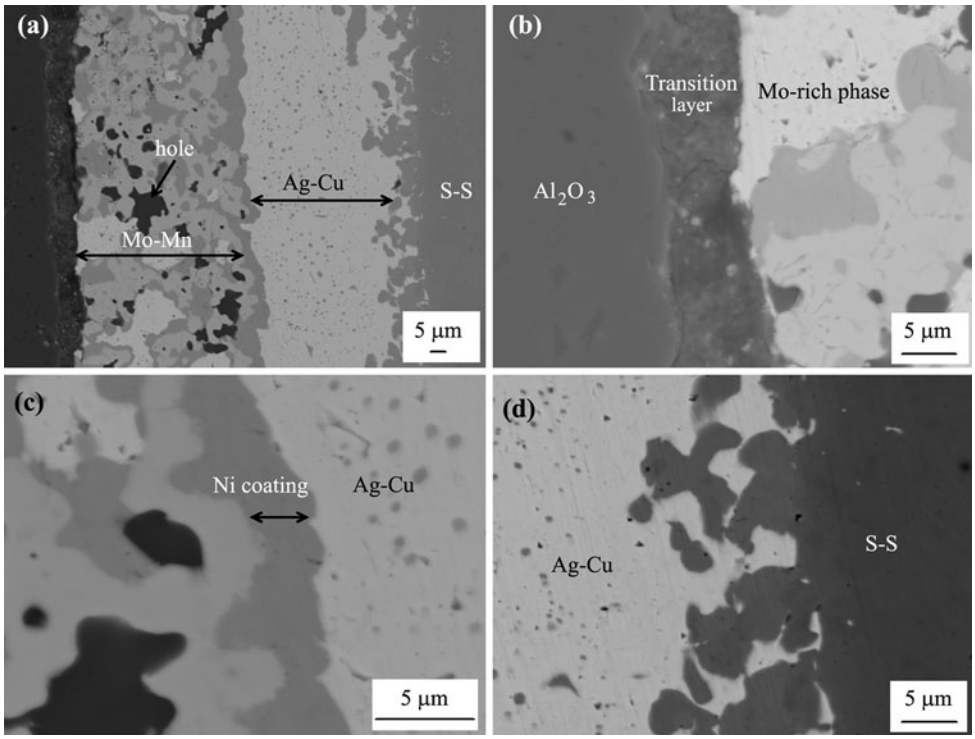

Fig. 6 BSE images of typical joint cross section (a) Al_2O_3/S-S section, (b) Al_2O_3/Mo-Mn interface, (c) Mo-Mn/Ni/Ag-Cu interface, and (d) Ag-Cu/S-S interface

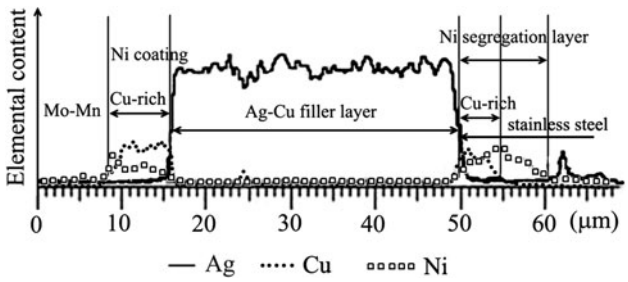

Fig. 7 Elemental EDS profiles across brazing filler layer, showing enrichment of Cu and separation of Ni

volatilized faster than Cu during vacuum brazing (a thin Ag deposition layer was found on the inner surface of the viewing window glass). This is because the saturated vapor pressure of Ag is smaller than that of Cu, as demonstrated by subsequent heat-treatment experiments. In these experiments, the joints were placed in the vacuum furnace ($\sim 8 \times 10^{-3}$ Pa) at 600 °C for 1-10 h. It was found that the longer the holding time was, the more visible the copper color on the exposed filler surface was. Another possible reason was the mutual attraction of Ni and Cu during vacuum brazing due to their similar atomic radius, resulting in the formation of Cu-Ni substitutional solid solution, which could explain the appearance of Ni segregation at the Ag-Cu/S-S interface (Fig. 7). Consequently, the thin Ni coating can prevent the Ag-Cu filler from entering the Mo-Mn layer, and even stop the Ag entering into itself to avoid eroding the Mo-Mn layer according to the EDS results. Furthermore, the Ni coating helped the alloy wet the rough surface of the metallized ceramic during brazing. Therefore, the thin Ni coating played a pivotal role in the bonding of the metallized Al_2O_3 ceramic to stainless steel via the Ag-Cu filler layer.

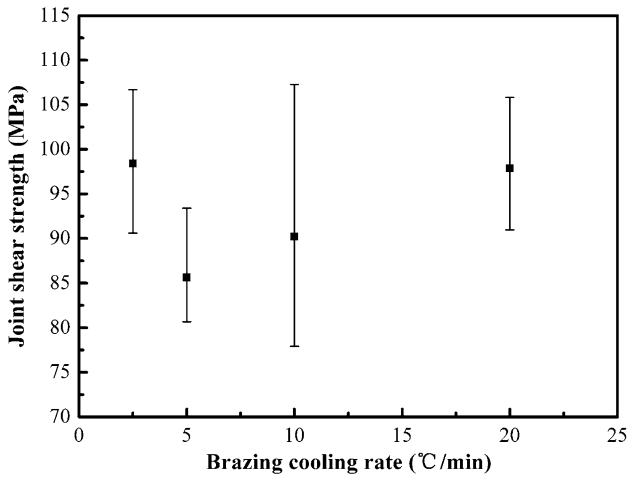

Fig. 8 Joint shear strength at different brazing cooling rates

3.3 Joint Shear Properties

Under the present experimental conditions, while the maximum cooling rate was set at ~20 °C/min, the actual cooling rate was less than 10, 5, and 2.5 °C/min at the furnace temperature of 600, 300, and 200°C, respectively, as the furnace (High-multi 5000, Japan) used was thermally well insulated. Thus, the furnace cooling mode was adopted when the actual cooling rate was less than that prescribed.

Figure 8 plots the measured joint shear strength as a function of brazing cooling rate. It can be seen from Fig. 8 that, under the present conditions, the brazing cooling rate did not significantly influence the joint shear strength, which varied between 80 and 110 MPa. It is possible that the interlayer

Fig. 9 Shear fracture surfaces of Al_2O_3 ceramic/stainless steel brazed joints

residual thermal stresses did not vary significantly with varying cooling rate, leading to similar joint strength. In fact, the actual cooling rates measured at relatively low temperatures (≤300 °C) were only slightly different, and it is known that the cooling rate at low temperatures can significantly affect the thermal residual stresses. Both the maximum strength of about 110 MPa and the relatively high-average strength (>95 MPa) were achieved at 2.5 °C/min.

The ceramic/metal joint strength can be mainly determined by the joining process and the characteristics of two components. As the two joining materials differ markedly in CTE, 7.4×10^{-6}/°C for Al_2O_3 and 18.5×10^{-6}/°C for S-S, the joint strength achieved thus far was rather limited (maximum 110 MPa).

It was found during the shear strength measurement that most of the joint fractures occurred in the ceramic matrix, only a few in the Mo-Mn layer, and none in the brazing filler layer (Fig. 9). This may be attributed to the fact that, in a typical ceramic-metal brazed joint, the metal and ceramic components experience compressive and tensile residual stresses, respectively, and the maximum thermal residual stress appeared in the ceramic matrix adjacent to the ceramic/Mo-Mn interface (Ref 14-17).

The influence of vacuum heat treatment at 600 °C for 1-10 h after brazing on joint shear strength was also investigated. The results (not shown here for brevity) demonstrated that the process had negative effect on the joint shear strength (only ~50 MPa). This can be attributed to the excessive volatilization of Ag that resulted in the more serious enrichment of Cu, which served to increase the interlayer residual thermal stresses.

4. Conclusions

High-purity Al_2O_3 ceramic/stainless steel joints were fabricated by activated Mo-Mn process with Ag-Cu filler metal. While a transition layer was formed between the ceramic matrix and the Mo-Mn metallizing layer, the glassy phases migrated mainly from the Mo-Mn layer to the ceramic matrix. The $MnAl_2O_4$ phase was produced in both the Mo-Mn layer and the sintered body of metallizing formula powder due to the existence of active agent (MnO and Al_2O_3). Glassy phase migration and chemical reaction in the activated Mo-Mn metallization of high-purity Al_2O_3 ceramic were experimentally confirmed as the two main bonding mechanisms. The Cu element was rich on both sides of the Ag-Cu filler layer, and the Ni element separated at the Ag-Cu/S-S interface. The thin Ni coating played a key role in the bonding of the metallized ceramic to stainless steel via the Ag-Cu filler layer. The maximum joint shear strength of about 110 MPa and average strength of over 95 MPa were attained. While the brazing cooling rate had small effect on the joint strength, the influence of vacuum heat treatment was significant.

Acknowledgments

This work is supported by the National Natural Science Foundation of China (51002114, 10825210), the National Basic Research Program of China (2011CB610305), the National 111 Project of China (B06024), the "13115" project of Shaanxi Province (S2010ZDKG704), and the Postdoctoral Science Foundation of China (20100470089).

References

1. P. Mishra, P. Sengupta, S.N. Athavale, A.L. Pappachan, A.K. Grover, A.K. Suri, G.B. Kale, P.K. De, and K. Bhanumurthy, Brazing of Hot Isostatically Pressed-Al_2O_3 to Stainless Steel (AISI, 304L) by Mo-Mn Route Using 72Ag-28Cu Braze, *Metall. Mater. Trans. A*, 2005, **36**(6), p 1487–1494
2. M.C.A. Nono, J.J. Barroso, and P.J. Castro, Mechanical Behavior and Microstructural Analysis of Alumina-Titanium Brazed Interfaces, *Mater. Sci. Eng. A*, 2006, **435–436**, p 602–605
3. G.W. Liu, G.J. Qiao, H.J. Wang, Z.H. Jin, and T.J. Lu, Joining of High Purity Al_2O_3 to Stainless Steel by Activated Molybdenum-Manganese Process, *Rare Met. Mater. Eng.*, 2007, **36**(5), p 920–923 (in Chinese)
4. S.H. Yang and S. Kang, Fracture Behavior Reliability of Brazed Alumina Joints Via Mo-Mn Process and Active Metal Brazing, *J. Mater. Res.*, 2000, **15**(10), p 2238–2243
5. R. Asthana and M. Singh, Joining of Partially Sintered Alumina to Alumina, Titanium, Hastealloy and C-SiC Composite Using Ag-Cu Brazes, *J. Eur. Ceram. Soc.*, 2008, **28**(3), p 617–631
6. Y. Iino, Partial Transient Liquid Phase Metals Layer Technique of Ceramic-Metal Bonding, *J. Mater. Sci. Lett.*, 1990, **9**(10), p 104–106
7. C.G. Zhang, G.J. Qiao, and Z.H. Jin, Active Brazing of Pure Alumina to Kovar Alloy Based on the Partial Transient Liquid Phase (PTLP) Technique with Ni-Ti Interlayer, *J. Eur. Ceram. Soc.*, 2002, **22**(13), p 2181–2186
8. A.G. Pincus, Metallographic Examination of Ceramic-Metal Seals, *J. Am. Ceram. Soc.*, 1953, **36**(5), p 152–158
9. S.S. Cole and G. Sommer, Glass-Migration Mechanism of Ceramic-to-Metal Seal Adherence, *Am. Ceram. Soc.*, 1961, **44**(6), p 265–271
10. M.E. Twentyman, High Temperature Metallizing, Part 1, The Mechanism of Glass Migration in the Production of Metal-Ceramic Seal, *J. Mater. Sci.*, 1975, **10**(55), p 765–776
11. L.Q. Gao, *The Practical Technology of Ceramic-Metal Seals*, Chemical Industry Press, Beijing, 2005, p 70–155 (in Chinese)
12. C.S. Li and D.B. Huang, *Handbook of Materials for Mechanical Engineering*, Electronic Industry Press, Beijing, 2006, p 453 (in Chinese)
13. G.W. Liu, G.J. Qiao, H.J. Wang, J.F. Yang, and T.J. Lu, Pressureless Brazing of Zirconia to Stainless Steel with Ag-Cu Filler Metal and TiH_2 Powder, *J. Eur. Ceram. Soc.*, 2008, **28**(14), p 2701–2708
14. L. Pintschovius, N. Pyka, R. Kussmaul, D. Munz, B. Elgenmann, and B. Scholtes, Experimental and Theoretical Investigation of the Residual Stress Distribution in Brazed Ceramic-Steel Components, *Mater. Sci. Eng. A*, 1994, **177**(1–2), p 55–61
15. X.L. Wang, C.R. Hubbard, S. Spooner, S.A. David, B.H. Rabin, and R.L. Williamson, Mapping of the Residual Stress Distribution in a Brazed Zirconia-Iron Joint, *Mater. Sci. Eng. A*, 1996, **211**(1–2), p 45–53

16. H. Chang, S.W. Park, S.C. Choi, and T.W. Kim, Effects of Residual Stress on Fracture Strength of Si_3N_4/Stainless Steel Joints with a Cu-Interlayer, *J. Mater. Eng. Perform.*, 2002, **11**(6), p 640–644

17. A. Kar, M. Ghosh, A.K. Ray, and A.K. Ray, Effect of Interfacial Thickness and Residual Stress on the Mechanical Property of the Alumina-Stainless Steel Braze Joint Interface, *Mater. Sci. Eng. A*, 2008, **498**(1–2), p 283–288